Available online at www.sciencedirect.com
SCIENCE DIRECT®
Journal of Solid State Chemistry 177 (2004) 1905–1911
JOURNAL OF SOLID STATE CHEMISTRY
http://elsevier.com/locate/jssc

Structure and Raman scattering study on $Ba_8Ga_xSi_{46-x}$ ($x = 10$ and 16) type I clathrates

Devaraj Nataraj*,[1] and Jiro Nagao

Institute for Energy Utilization, National Institute of Advanced Industrial Science and Technology (AIST), 2-17-2-1 Tsukisamu Highashi, Toyohira, Sapporo 062-8517, Japan

Received 1 October 2003; received in revised form 7 January 2004; accepted 16 January 2004

Abstract

Structure and vibrational properties of $Ba_8Ga_xSi_{46-x}$ ($x = 10$ and 16) clathrates were studied by X-ray diffraction and Raman scattering measurements. The temperature dependent electrical resistivity measurement on $Ba_8Ga_{10}Si_{36}$ has shown semiconducting nature of that clathrate with an energy band gap value of 0.31 eV. On the other hand the measurement on $Ba_8Ga_{16}Si_{30}$ has shown metallic like electrical conductivity of that clathrate. The origin of semiconductivity in $Ba_8Ga_{10}Si_{36}$ was found to be due to the vacancy disorder in the framework sites. Room temperature Raman scattering measurements resolved several Raman vibrational modes, including low frequencies ones corresponding to the rattling motion of Ba atoms. The low frequency positions of Ba in the respective clathrates at 49.4, 73.7 and 97.3 cm^{-1} for $Ba_8Ga_{10}Si_{36}$ and at 43.7, 74.5 and 92.4 cm^{-1} for $Ba_8Ga_{16}Si_{30}$ were found to be in agreement with the reported density functional (DF) calculated low frequency modes of $Ba_8Ga_{16}Si_{30}$. The framework gallium difference and vacancy disorders were found to influence the position and widths of frequency modes. Room temperature lattice thermal conductivity of $Ba_8Ga_{10}Si_{36}$ and $Ba_8Ga_{16}Si_{30}$ were 1.128 and 1.071 $Wm^{-1}K^{-1}$, respectively, and this low value was attributed to the resonant scattering between the framework acoustic and Ba rattling modes.

Keywords: Si clathrates; Raman scattering; Semiconducting clathrates; Cage like structure

1. Introduction

Tetrahedral atoms silicon, germanium and tin form cage like framework structure enclosing alkali or alkaline metal atoms [1–3]. These cage-like materials, also known as clathrates, were found to have a wide variety of electronic behaviors, including superconductivity in Ba_8Si_{46} [4] and ferromagnetism in $Ba_8Mn_2Ge_{44}$ [5]. Recently there has been considerable interest in these materials due to their potential application in thermoelectric cooling [6–8]. The unit cell of type I clathrate consists of two dodecahedral (cages with 20 atoms; small cage) and six tetrakaidecahedral cages (cages with 24 atoms; large cage), the center of which is occupied by alkali or alkaline metal atoms. The crystallographic location of the tetrahedral atoms is 6*c*, 16*i* and 24*k*, and that of the caged atoms is 2*a* and 6*d*, respectively. Fig. 1 shows the dodecahedral and tetrakaidecahedral cages of the type I clathrate structure. The interaction between the caged (guest) and framework atoms (host) is weak and therefore the rattling frequency of the guest atom is localized and this localized rattling motion is reported to be responsible for the lowering of lattice thermal conductivity in various clathrates, because of their resonant scattering with the acoustic phonon modes of the framework atoms. Experimental investigation on various clathrates have shown low room temperature lattice thermal conductivity, for example that of $Ba_8Ga_{16}Ge_{30}$ [9] and $Sr_8Ga_{16}Ge_{30}$ [10] were 1.3 and 0.9 $Wm^{-1}K^{-1}$, respectively. Though lattice thermal conductivity of clathrate compound is lowered by Ba rattling modes, the electrical conductivity is not much affected and therefore it has potential application in the field of thermoelectrics.

Reports are available on the transport and thermoelectric properties of clathrates. The electrical resistivity measurements on various Si and Ge clathrate have shown that they are metallic because of their heavily

*Corresponding author. Fax: +81-11-716-6004.
E-mail address: d.nataraj@lycos.com (D. Nataraj).
[1] Present address: Research Center for Integrated Quantum Electronics, Hokkaido University, North 13 West 8, Sapporo, Hokkaido 060-8628, Japan.

0022-4596/$ - see front matter © 2004 Elsevier Inc. All rights reserved.
doi:10.1016/j.jssc.2004.01.011

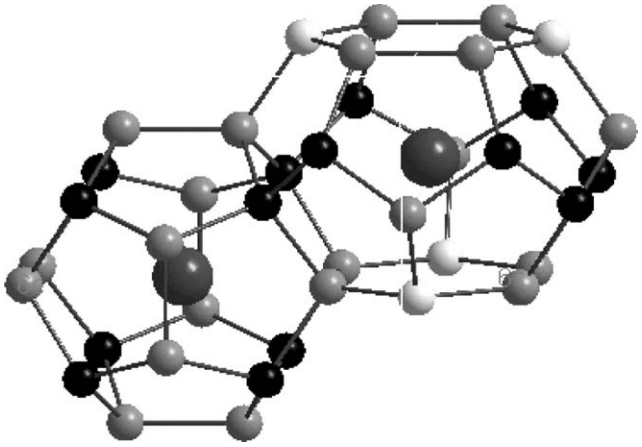

Fig. 1. Small and large cages of type I clathrate structure (White atoms are 6*c* position; light gray atoms are 16*i* position; dark atoms are 24*k* position; the central big atoms are Ba position).

doped nature. Very few semiconducting clathrates have only been reported. The reduction in the carrier concentration due to excess gallium at the framework sites or framework vacancies was found to lead to the semiconducting nature in those clathrates. Nolas et al. [11] have introduced excess gallium at the framework sites of $Sr_8Ga_{16-x}Ge_{30-y}$ and obtained semiconducting behavior in that clathrate. Ramachandran et al. [12] and Hermann et al. [13] have found vacancy induced semiconducting behavior in K_8Ge_{46} and Ba_8Ge_{46} clathrates, respectively.

Though various reports are available on $Ba_8Ga_{16}Si_{30}$ clathrates [14,15], no report is available on the vibrational properties of these clathrates. Therefore in the present article we report a detailed investigation on the vibrational properties of $Ba_8Ga_xSi_{46-x}$ clathrates. The effect of change in gallium concentration on the structure, transport and vibrational properties are studied and the results are discussed.

2. Experimental details

Stoichiometric amounts of constituent elements (pure Ba, Ga and Si) were melted in an argon atmosphere by an Ar ion gun to get $Ba_8Ga_{10}Si_{36}$ and $Ba_8Ga_{16}Si_{30}$ clathrates. The chemical composition of the as prepared samples was analyzed by electron probe microanalysis (EPMA). Powder X-ray (Cu$K\alpha$) diffraction data collected in the range of $2\theta = 10-70^\circ$, with step of 0.02°, showed characteristic type-I clathrate reflections of the as prepared samples. Structure refinements were carried out using Rietveld refinement program visual RIETAN by Izumi [16,17]. Background coefficients, scale factors, peak shapes (pseudo Voigt), atomic coordinates, unit cell constants, isotropic thermal parameters and site occupancies were all refined. Cold pressed and consequently annealed samples, with a theoretical density of 94%, were used for the transport and thermal conductivity measurements. The electrical resistivity (ρ) was measured in the temperature range of 300–850 K by van der Pauw technique. The carrier concentration was calculated from the measured Hall coefficient (R_H) by the relation $n = 1/R_H e$, where e is electric charge. The heat capacity and thermal diffusivity were measured using laser flash diffusive technique. Room temperature thermal conductivity (κ) was calculated from the measured experimental density (d), heat capacity (C_P) and thermal diffusivity (D) by the relation ($\kappa = DC_Pd$). Raman scattering measurements were done on bulk samples using the 514.5 nm excitation of argon ion laser. Due to low thermal conductivity of the sample, the power of incident beam onto the sample was limited to 50 mW.

3. Results and discussion

3.1. Structural details

Figs. 2(a) and (b) shows the XRD pattern of $Ba_8Ga_{10}Si_{36}$ and $Ba_8Ga_{16}Si_{30}$ clathrates showing char-

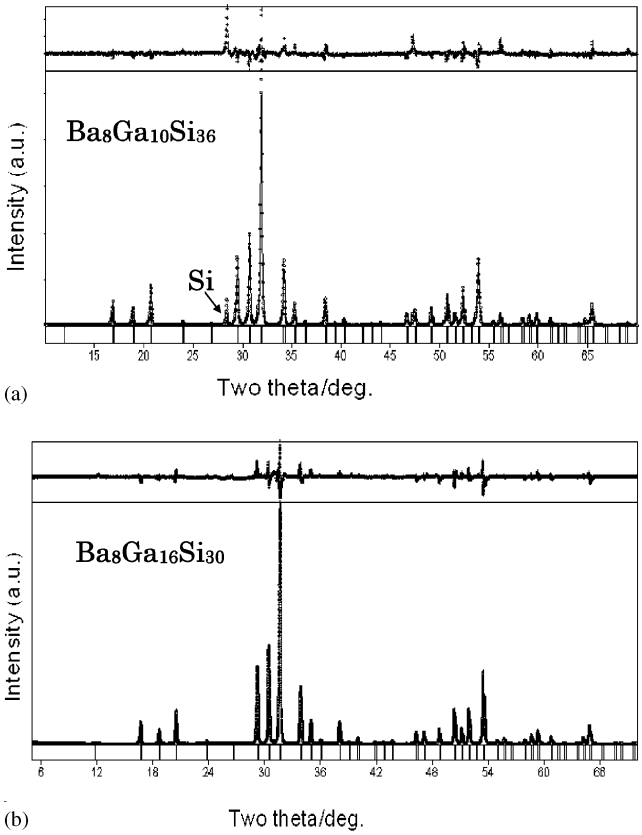

Fig. 2. (a, b) Rietveld analysis of the X-ray diffraction pattern of (a) $Ba_8Ga_{10}Si_{36}$ and (b) $Ba_8Ga_{16}Si_{30}$ clathrates. Experimental data points are shown as dots and theoretical fits are shown as solid curves. Tick marks below the fit corresponds to the position of the Bragg reflections expected for the structure. Curve shown above the fit is the difference between the observed and theoretical patterns.

Table 1
Rietveld fitting parameters of $Ba_8Ga_{10}Si_{36}$ and $Ba_8Ga_{16}Si_{30}$ clathrates

Sample	Atoms	Site	x	y	z	U_{iso} (Å^2)
$Ba_8Ga_{10}Si_{36}$	Ba1	2*a*	0	0	0	0.0097(1)
	Ba2	6*d*	0.25	0.5	0	0.0278(6)
	Si1	6*c*	0.25	0	0.5	0.0070(9)
	Si2	16*i*	0.1848(1)	0.1848(1)	0.1848(1)	0.0096(5)
	Si3	24*k*	0	0.3062(9)	0.1192(8)	0.0092(9)
$Ba_8Ga_{16}Si_{30}$	Ba1	2*a*	0	0	0	0.0081(6)
	Ba2	6*d*	0.25	0.5	0	0.0181(3)
	Si1	6*c*	0.25	0	0.5	0.0078(2)
	Si2	16*i*	0.1850(2)	0.1850(2)	0.1850(2)	0.0090(6)
	Si3	24*k*	0	0.3073(6)	0.1192(6)	0.0083(4)
Reliability factors*						
For $Ba_8Ga_{10}Si_{36}$ $R_{wp} = 0.1114$,	$R_p = 0.0832$, $S(= R_{wp}/R_e) = 1.755$					
For $Ba_8Ga_{16}Si_{30}$ $R_{wp} = 0.1121$,	$R_p = 0.0820$, $S(= R_{wp}/R_e) = 1.943$					

*R_{wp}: R weighted pattern, R_e: R expected, S: goodness of fit.

Table 2
List of refined interatomic distances (Å) and angles (deg) for $Ba_8Ga_{10}Si_{36}$ and $Ba_8Ga_{16}Si_{30}$ clathrates

		$Ba_8Ga_{10}Si_{36}$	$Ba_8Ga_{16}Si_{30}$			$Ba_8Ga_{10}Si_{36}$	$Ba_8Ga_{16}Si_{30}$
Distance (Si–Si)	Si1–4Si3[a]	2.452	2.461	Distance (Ba–Si)	Ba1–Si2	3.357	3.373
	Si2–1Si2	2.368	2.369		Ba1–Si3	3.445	3.459
	Si2–3Si3	2.418	2.429		Ba2–Si1	3.708	3.722
	Si3–1Si3	2.502	2.510		Ba2–Si3	3.546	3.558
	Si3–2Si2	2.418	2.429		Ba2–Si3	4.038	4.052
	Si3–1Si1	2.452	2.261		Ba2–Si2	3.892	3.906
Angles on Si1	Si3–Si1–Si3	108.21	108.24	Angles on Si3	Si1–Si3–Si2	106.10	106.01
	Si3–Si1–Si3	112.03	111.96		Si1–Si3–Si3[b]	123.98	124.02
Angles on Si2	Si2–Si2–Si3	108.86	108.58		Si2–Si3–Si2	106.56	106.59
	Si3–Si2–Si3	110.08	110.02		Si2–Si3–Si3	106.51	106.57

Ba1, Ba2, Si1, Si2 and Si3 are crystallographic positions in type I clathrate structure respectively for 2*a*, 6*d*, 6*c*, 16*i* and 24*k* positions.
[a] The numbers before the atomic position represents the multiplicity.
[b] Six ring angle.

acteristic type-I clathrate reflections of the as prepared samples. A detailed quantitative measure of framework site occupancy and the thermal parameters of atoms were obtained by Rietveld refinement of the X-ray powder data. Table 1 shows the refined data. The refined lattice parameters of $Ba_8Ga_{10}Si_{36}$ and $Ba_8Ga_{16}Si_{30}$ were 1.0474 and 1.0526 nm, respectively. The observed difference in the lattice constant can be attributed to the difference in the number of Si–Ga bonds in the respective clathrates. As the Ga concentration increases the number of Si–Ga bonds, with slightly longer bond lengths than that of Si–Si, increases and as a result the lattice parameter and the interatomic distance between the guest and host framework of $Ba_8Ga_{16}Si_{30}$ increases. The lattice constant value of Ba_8Si_{46} is 1.0192 nm, which is lower than that of $Ba_8Ga_{10}Si_{30}$ and $Ba_8Ga_{16}Si_{36}$ clathrates also support the fact that the difference in the number of Si–Si/Si–Ga bond determines the lattice parameter. The interatomic distance between Ba and framework atoms of the respective clathrates were calculated from the refined data and tabulated in Table 2.

The refined results gave the total occupancy of Ga/Si equal to 3.492(9)/2.012(2), 0.993(2)/14.012(8), and 5.512(8)/17.986(7) for $Ba_8Ga_{10}Si_{36}$ and 3.995(2)/2.005(8), 1.994(5)/14.007(1), and 10.006(8)/13.999(2) for $Ba_8Ga_{16}Si_{30}$, respectively, for 6*c*, 16*i*, and 24*k* sites. Similarly, the refined total occupancy of Ba at the 2*a* and 6*d* sites are 1.987(9) and 5.976(9) for $Ba_8Ga_{10}Si_{36}$ and 1.972(6) and 6.00 for $Ba_8Ga_{16}Si_{30}$, respectively. Therefore according to the refined occupational factors, the calculated composition of the respective clathrates is $Ba_{7.96}Ga_{10}Si_{34.01}$ ($Ba_{7.8}Ga_{10}Si_{34}$) and $Ba_{7.97}Ga_{16}Si_{30}$ ($Ba_{7.9}Ga_{16}Si_{30}$) (the composition values given in the brackets are from the experimental electron probe microanalysis). The occupancies of $Ba_8Ga_{10}Si_{36}$ indicates that there are vacancies at 6*c*, 16*i*, and 24*k* sites of $Ba_8Ga_{10}Si_{36}$, with one vacancy at 16*i* and fraction of one vacancy at 6*c* and 24*k* sites respectively.

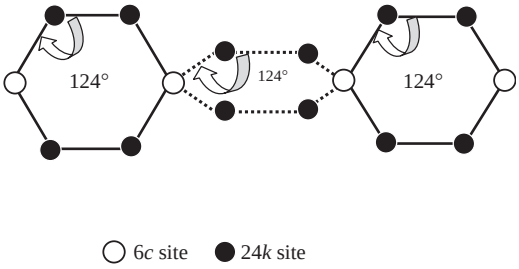

Fig. 3. Six ring region of type I clathrate structure.

In general the vacancy formation preferably occurs in the six ring region. This is because the six ring region is under stress due to large deviation in the tetrahedral angle of that region, and this stress is released by the creation of vacancies. Fig. 3 shows the six ring region of the type I clathrate structure, in which the angle on the atoms in 24*k* site is about 124°, i.e., 12% greater than that of cubic diamond silicon structure. Though the entire six ring region is under stress, the vacancy formation is preferred at the 6*c* site rather than the 24*k* site of that region. This is because the 6*c* site is shared by tetrakaidecahedral cages only, whereas the 24*k* site is shared by both dodecahedral and tetrakaidecahedral cages. As the deviation of tetrahedral angle in the tetrakaidecahedral cages are relatively higher than that in dodecahedral cages (Table 2), the 6*c* sites which are shared by tetrakaidecahedral cages alone are preferred in the vacancy formation process. The 6*c* site vacancy formation was observed in binary clathrates like Ba_8Ge_{46} and K_8Ge_{46} [12,13]. In contrast, silicon binary clathrate Ba_8Si_{46} has shown no 6*c* site vacancy [18]. The reason is that Ge–Ge bonds are weak and therefore the 6*c* site vacancy formation is an energetically favorable process in Ba_8Ge_{46} and K_8Ge_{46} clathrates, and not favorable in Ba_8Si_{46} clathrate. However, when gallium is doped, all the binary clathrates including germanium clathrates have shown no vacancies at the 6*c* site [15], and this is due to the preferential occupation of gallium at these sites.

In contrast to the above discussion, Rietveld refinement results on $Ba_8Ga_{10}Si_{36}$ have shown vacancies at all framework sites. As the vacancies are distributed almost randomly at all framework sites, it is believed that the deviation in the stoichiometric requirement of 16 gallium per unit cell of that clathrate is the reason for the observed random distribution, which is consistent with the recent theoretical calculations on the stability of the type I clathrate structure [19].

3.2. Electrical properties

Fig. 4 shows the temperature dependence of electrical resistivity (ρ) in the temperature range of 300–850 K for $Ba_8Ga_{10}Si_{36}$ and $Ba_8Ga_{16}Si_{30}$ clathrates, with room temperature carrier concentration of 3.02×10^{19} and $1.41\times10^{21}\,cm^{-3}$, respectively. The temperature dependant ρ indicates semiconducting behavior of $Ba_8Ga_{10}Si_{36}$ clathrate, whereas that of $Ba_8Ga_{16}Si_{30}$ is like a heavily doped semiconductor. From the slope of the graph drawn between $1000/T$ versus ρ, in the high temperature region, the energy band gap value of $Ba_8Ga_{10}Si_{36}$ was estimated as 0.31 eV. This value is close to the theoretical value of 0.4 eV calculated by density functional theory on $Ba_8Ga_{16}Si_{30}$ clathrate [20]. As the framework gallium doping determines the Fermi level shift, rather than the energy band gap value, the value of 0.31 eV could be the energy band gap value of $Ba_8Ga_{16}Si_{30}$ clathrate.

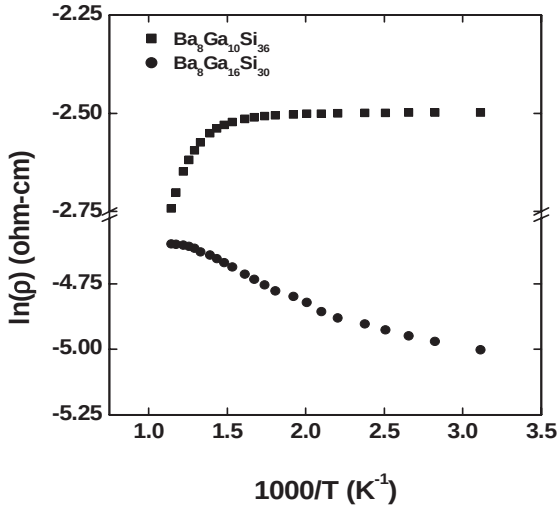

Fig. 4. Electrical resistivity as a function of temperature for $Ba_8Ga_{10}Si_{36}$ and $Ba_8Ga_{16}Si_{30}$ clathrates.

In general clathrate compounds having no vacancies at their framework site show metallic like electrical conductivity because of their heavily doped nature. In contrast, the electrical resistivity of clathrate with vacancies at the framework sites shows semiconducting behavior due to the reduction of conduction band population followed by the occupation of guest valence electrons at vacancy induced defect states. Hall measurements show decreasing carrier concentration of $Ba_8Ga_{10}Si_{36}$ clathrate followed by occupation of electrons at the defect states.

3.3. Raman spectroscopy

Figs. 5(a) and (b) shows Raman scattering spectra of $Ba_8Ga_{10}Si_{36}$ and $Ba_8Ga_{16}Si_{30}$ clathrates. The result of Lorentzian curve fitting is also shown in the figure with the experimental data represented as dots. In the present case the experimental Raman scattering measurements resolved 17 and 15 modes respectively for $Ba_8Ga_{10}Si_{36}$ and $Ba_8Ga_{16}Si_{30}$ clathrates. The high frequency mode for the respective clathrates is at 489.2 and 512.5 cm^{-1}. The high frequency phonon mode of $Ba_8Ga_{16}Si_{30}$ at

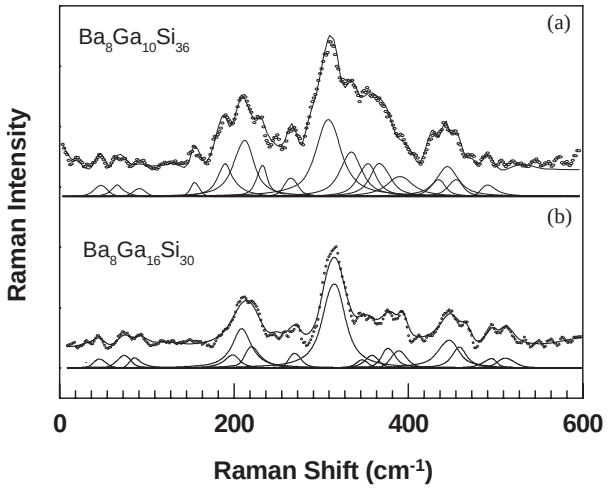

Fig. 5. (a, b) Raman scattering spectra of $Ba_8Ga_{10}Si_{36}$ and $Ba_8Ga_{16}Si_{30}$ clathrates at $T = 300\,K$. The data are represented by the points and the solid lines are fit to the spectrum.

Table 3
Raman frequency (ω) and line width (Γ) details of $Ba_8Ga_{10}Si_{36}$ and $Ba_8Ga_{16}Si_{30}$ clathrates

$Ba_8Ga_{10}Si_{36}$		$Ba_8Ga_{16}Si_{30}$	
ω (cm^{-1})	Γ (cm^{-1})	ω (cm^{-1})	Γ (cm^{-1})
49.4	9.1	43.7	7.1
73.7	15.5	74.5	13.0
97.3	12.9	92.4	14.2
157.4	9.7		
191.1	17.5	190	7.4
213.7	21.2	208.7	21.5
232.2	8.4	224	16.1
269.2	11.3	272.2	7.9
312.8	20.9	314.6	25.2
334.9	21.8	346.5	7.8
352.7	14.9	357.3	12.8
365.5	20.7	376.9	15.5
392.7	17.9	392.9	9.8
427.5	13.2		
440.5	15.2	446.4	23.3
453.1	10.0	466.3	8.6
489.2	7.5	494.5	11.6

$512.5\,cm^{-1}$ corresponds to small amount of possible silicide phase present in the sample. Similar types of modes corresponding to the silicide phase are observed in $Ca_{1-x}La_xSi_2$ silicide and in $K_{2.9}Ba_{4.9}Si_{46}$ clathrate [21]. Table 3 shows the frequency position and line width information obtained from Lorentzian curve fitting. To correlate the frequency position with the possible vibrational modes, the experimental frequency modes were compared with those theoretically calculated by various authors [22–24]. The comparison has shown that the frequency positions are not in agreement and the reason for this may be due to the fact that the theoretical frequencies were from empty Si_{46} clathrate, whereas the experimental results are from Ba containing Si_{46} clathrate. Room temperature Raman scattering spectra of silicon clathrates like Na_8Si_{46}, K_7Si_{46}, $K_{2.9}Ba_{4.9}Si_{46}$ and $Na_{0.2}Ba_{5.6}Si_{46}$ were also similar to our Raman results and not in agreement with theoretical data [21]. Therefore, it seems that a more sophisticated theory, including the structural relaxation, charge transfer between Ba and framework atoms and consequent interaction among themselves appear to be necessary to quantitatively understand the experimental data.

Most of the line widths of frequency modes of $Ba_8Ga_{10}Si_{36}$ are relatively broader than that of $Ba_8Ga_{16}Si_{30}$ and this broadening is due to vacancy disorder distributed at the framework sites of $Ba_8Ga_{10}Si_{36}$. As the vacancy disorder terminates the spatial extension of phonons, the $q = 0$ condition requiring infinite spatial extension of phonon waves, according to $q = 2\pi/\lambda = 0$, is violated and because of this violation phonons with non-zero wave vectors are produced and contribute to the line width broadening.

From Table 3 it can also be seen that most of the optical phonon modes of $Ba_8Ga_{10}Si_{36}$ were relatively red shifted with respect to that of $Ba_8Ga_{16}Si_{30}$, and this red shift is due to the difference in the lattice parameter of the respective clathrates. The lattice parameter of $Ba_8Ga_{10}Si_{36}$ has smaller magnitude than that of $Ba_8Ga_{16}Si_{30}$ and therefore the interatomic distance between Ba and framework atoms is reduced in $Ba_8Ga_{10}Si_{36}$. As a result, there is a relatively strong interaction between Ba and framework atoms of $Ba_8Ga_{10}Si_{36}$ and this strong interaction weakens the framework bond strength leading to the red shift of most of the optical phonon modes of $Ba_8Ga_{10}Si_{36}$.

The frequency region below $100\,cm^{-1}$ has three peaks, centered at 49.4, 73.7 and $97.3\,cm^{-1}$ for $Ba_8Ga_{10}Si_{36}$ and at 43.7, 74.5 and $92.4\,cm^{-1}$ for $Ba_8Ga_{16}Si_{30}$, respectively. The peak positions of these low frequency modes are comparable with the DF calculated Raman frequency modes of $Ba_8Ga_{16}Si_{30}$ at 40.82, 73.76 and $101.66\,cm^{-1}$ [18]. Therefore, according to the comparison, the modes of $Ba_8Ga_{10}Si_{36}$ at 49.4 and $73.7\,cm^{-1}$ and that of $Ba_8Ga_{16}Si_{30}$ at 43.7 and $74.5\,cm^{-1}$ were attributed to the rattling motion of Ba in large cages, respectively, in two different directions parallel and perpendicular to the plane of the six ring. Similarly the other modes of the respective clathrates at 97.3 and $92.4\,cm^{-1}$ were attributed to the rattling motion of Ba in small cages.

4. Thermal property

As the Ba rattling modes, with their frequency of vibrations in acoustic range can resonantly scatter the

Table 4
Thermodynamic related parameters of $Ba_8Ga_{10}Si_{36}$ and $Ba_8Ga_{16}Si_{30}$ clathrates estimated from room temperature X-ray crystallographic data

Sample	$Ba_8Ga_{10}Si_{36}$	$Ba_8Ga_{16}Si_{30}$
Θ_D (K)	352.17	346.25
υ_s (m/S)	3311	3237
d (nm)	0.5237	0.5263
$\kappa_{lattice}$ ($Wm^{-1}K^{-1}$) (calc.)	0.918	0.923
$\kappa_{lattice}$ ($Wm^{-1}K^{-1}$)(exp.)	1.128	1.071

acoustic phonons from the framework atoms, the lattice thermal conductivity of these clathrates is low. Experimental room temperature lattice thermal conductivity ($\kappa_{lattice}$) values of $Ba_8Ga_{10}Si_{36}$ and $Ba_8Ga_{16}Si_{30}$ clathrates are low with a magnitude of 1.128 and 1.071 $Wm^{-1}K^{-1}$, respectively and this low value could be an experimental support of rattling contribution. The $\kappa_{lattice}$ was deduced from the experimentally obtained total thermal conductivity (κ), by the relation $\kappa_{lattice} = \kappa - L_0 T/\rho$, where L_0 is Lorenz number ($L_0 = 2.44 \times 10^{-8}\,W\Omega K^{-2}$), T is temperature and ρ is resistivity.

The experimental $\kappa_{lattice}$ values were found to be similar to that of the theoretical values calculated from the room temperature X-ray data by a method described elsewhere [25]. The calculated values were obtained from room temperature X-ray diffraction data by the relation $\kappa_{lattice} = 1/3 C_v \upsilon_s d$, where C_v is heat capacity per unit volume (25 J/mol/K), υ_s is velocity of sound and d is mean free path of the phonons. The velocity of sound was estimated from the Debye temperature, and Debye temperature in turn was estimated from the average isotropic atomic displacement parameter (U_{iso}) of the framework atoms of the respective clathrates as discussed elsewhere [25] (*in calculating the average U_{iso}, the contribution from Ba atoms was neglected assuming that they are localized*). The mean free path of the phonons were considered to be equal to the distance between two nearest neighbor Ba atoms in the tetrakaidecahedral cages, as the rattling motion of these atoms resonantly scatters the acoustic phonons in these clathrates. Table 4 summarizes various parameters calculated from the room temperature atomic displacement parameter values. The calculated and the experimental room temperature $\kappa_{lattice}$ values are in agreement and thus confirms our consideration that the framework atoms alone contribute to the heat capacity.

5. Conclusions

In conclusion, $Ba_8Ga_xSi_{46-x}$ ($x = 10$ and 16) clathrates were prepared by arc melting method and deviation in the stoichiometric requirement of 16 gallium atoms per unit cell of $Ba_8Ga_{16}Si_{30}$ was found to lead to a random framework vacancies, and consequently to the semiconducting nature of the clathrate. From the temperature dependent electrical resistivity measurements, the energy band gap value of $Ba_8Ga_{10}Si_{36}$ was estimated as 0.31 eV. Room temperature Raman scattering measurements resolved 17 and 15 vibrational modes, including localized Ba rattling modes. The line width broadening in the clathrates were found to be due to the contribution from disorders. The red shift of optical phonon modes of $Ba_8Ga_{10}Si_{36}$ was due to the relatively strong interaction between Ba and the framework atoms. Agreement between experimental and calculated lattice thermal conductivities confirmed the localization of Ba rattling modes.

Acknowledgments

The authors are grateful to Dr. H. Narita and Dr. T. Ebinuma of the AIST for useful discussions. One of the authors, D.N., would like to thank Science and Technology Agency of Japan (JISTEC-JST) for awarding a STA fellowship.

References

[1] B. Eisenmann, H. Schafer, R. Zakler, J. Less-Common Met. 118 (1986) 43.
[2] G.S. Nolas, T.J.R. Weakley, J.L. Cohn, R. Sharma, Phys. Rev. B 61 (2000) 3845.
[3] G.S. Nolas, B.C. Chakoumakos, B. Mahieu, G.J. Long, T.J.R. Weakley, Chem. Mater. 12 (2000) 1947.
[4] S. Yamanaka, E. Enishi, H. Fukuoka, Inorg. Chem. 39 (2000) 56.
[5] T. Kawaguchi, K. Tanigaki, M. Yasukawa, Appl. Phys. Lett. 77 (2000) 3438.
[6] J.L. Cohn, G.S. Nolas, V. Fessatidis, T.H. Metcalf, G.A. Slack, Phys. Rev. Lett. 82 (1999) 779.
[7] G.S. Nolas, in: T.M. Tritt, G. Mahan, H.B. Lyon Jr., M.G. Kanatzidis (Eds.), Thermoelectric Materials—The next generation Materials for Small Scal Refrigeration and Power Generation Applications, MRS Symposia Proceedings, Vol. 545, Materials Research Society, Pittsburgh, 1999, pp. 435–442.
[8] G. Slack, in: D.M. Rowe (Ed.), CRC Handbook of Thermoelectrics, CRC, Boca Raton, 1995, pp. 407–440.
[9] B.C. Sales, R.J. Chakoumakos, J.R. Thompson, D. Mandrus, Phys. Rev. B 63 (2001) 245113.
[10] J.L. Cohn, G.S. Nolas, V. Fessatidis, T.H. Metcalf, G.A. Slack, Phys. Rev. Lett. 82 (1999) 779.
[11] G.S. Nolas, J.L. Cohn, G.A. Slack, S.B. Schujman, Appl. Phys. Lett. 73 (1998) 178.
[12] G.K. Ramachandran, P.F. McMillan, J.J. Dong, O.F. Sankey, J. Solid State Chem. 154 (2000) 626.
[13] R.F.W. Herrmann, K. Tanigaki, T. Kawaguchi, S. Kuroshima, O. Zhou, Phys. Rev. B 60 (1999) 13245.
[14] D. Nataraj, J. Nagao, M. Ferhat, T. Ebinuma, J. Appl. Phys. 87 (2003) 2424.
[15] V.L. Kuznetzov, L.A. Kuznetsova, A.E. Kaliazin, D.M. Rowe, J. Appl. Phys. 87 (2000) 7871.

[16] F. Izumi, Rigaku J. 6 (1989) 10.
[17] F. Izumi, in: R.A. Young (Ed.), The Rietveld Method, Oxford Science Publications, Oxford, 2000, pp. 236–253.
[18] A. Kitano, K. Moriguchi, M. Yonemura, S. Munetoh, A. Shintani, H. Fukuoka, S. Yamanaka, E. Nishibori, M. Takata, M. Sakata, Phys. Rev. B 64 (2001) 45206.
[19] N.P. Blake, D. Bryan, S. Latturner, L. MØllnitz, G.D. Stucky, H. Metiu, J. Chem. Phys. 114 (2001) 10063.
[20] N.P. Blake, S. Latturner, J.D. Bryan, G.D. Stucky, H. Metiu, J. Chem. Phys. 115 (2001) 8060.
[21] S.L. Fang, L. Grigorian, P.C. Eklund, D. Dresselhaus, M.S. Dresselhaus, H. Kawaji, S. Yamanaka, Phys. Rev. B 57 (1998) 7686.
[22] M. Menon, E. Richter, K.R. Subbaswamy, Phys. Rev. B 56 (1997) 12290.
[23] R. Alben, D. Weaire, J.E. Smith Jr., M.H. Brodsky, Phys. Rev. B 11 (1975) 2271.
[24] Kahn, J.P. Lu, Phys. Rev. B 56 (1997) 13898.
[25] B.C. Sales, B.C. Chakoumakos, D. Mandrus, J.W. Sharp, J. Solid State Chem. 146 (1999) 528.